Conformational Changes in the Tryptophan Synthase from a Hyperthermophile upon $\alpha_2\beta_2$ Complex Formation: Crystal Structure of the Complex[†,‡]

Soo Jae Lee,[§] Kyoko Ogasahara,[§] Jichun Ma,[§] Kazuya Nishio,[§] Masami Ishida,[||] Yuriko Yamagata,[⊥] Tomitake Tsukihara,[§] and Katsuhide Yutani*[,#]

Institute for Protein Research, Osaka University, 3-2 Yamadaoka, Suita, Osaka 565-0871, Japan, Tokyo University Marine Science and Technology, 4-5-7 Kouonan, Minato-ku, Tokyo 108-8477, Japan, Graduate School of Pharmaceutical Sciences, Kumamoto University, 5-1 Oe-honmachi, Kumamoto 862-0973, Japan, and RIKEN Harima Institute at SPring8, 1-1-1 Kouto, Mikazuki-cho, Sayo-gun, Hyogo 679-5148, Japan

Received February 21, 2005; Revised Manuscript Received May 11, 2005

ABSTRACT: The three-dimensional structure of the bifunctional tryptophan synthase $\alpha_2\beta_2$ complex from *Pyrococcus furiosus* was determined by crystallographic analysis. This crystal structure, with the structures of an α subunit monomer and a β_2 subunit dimer that have already been reported, is the first structural set in which changes in structure that occur upon the association of the individual tryptophan synthase subunits were observed. To elucidate the structural basis of the stimulation of the enzymatic activity of each of the α and β_2 subunits upon $\alpha_2\beta_2$ complex formation, the conformational changes due to complex formation were analyzed in detail compared with the structures of the α monomer and β_2 subunit dimer. The major conformational changes due to complex formation occurred in the region correlated with the catalytic function of the enzyme as follows. (1) Structural changes in the β subunit were greater than those in the α subunit. (2) Large movements of A46 and L165 in the α subunit due to complex formation caused a more open conformation favoring the entry of the substrate at the α active site. (3) The major changes in the β subunit were the broadening of a long tunnel through which the α subunit product (indole) is transferred to the β active site and the opening of an entrance at the β active site. (4) The changes in the conformations of both the α and β subunits due to complex formation contributed to the stabilization of the subunit association, which is critical for the stimulation of the enzymatic activities.

Biological functions in living organisms are achieved by specific molecular recognition among many materials. In particular, protein−protein or protein−ligand interactions play a central role in physiological functions such as allosteric regulation. During these interactions, conformational changes in proteins, such as an induced-fit mode (*1*, *2*), are critically responsible for the functions (*3*−*7*). It is important to elucidate the structural changes in proteins coupled to the binding of the protein or ligand for solving the protein function mechanism. Tryptophan synthase is a paradigm for protein−protein interactions, protein−ligand interactions, and allosteric regulation induced by the binding of ligands (*8*−*12*). Bacterial tryptophan synthase is a bifunctional tetrameric enzyme ($\alpha_2\beta_2$ complex) that catalyzes the last two steps in the biosynthesis of L-tryptophan. The separate α and β_2 subunits catalyze two distinct reactions, termed the α and pyridoxal 5′-phoshate dependent β reactions (eqs 1 and 2), respectively. The $\alpha_2\beta_2$ complex catalyzes the sequential reactions of the two subunits, which is a physiologically important reaction termed the $\alpha\beta$ reaction (eq 3) (*8*).

α reaction

$$\text{indole 3-glycerol phosphate} \leftrightarrow \text{indole} + \text{D-glyceraldehyde 3-phosphate} \quad (1)$$

β reaction

$$\text{L-serine} + \text{indole} \rightarrow \text{L-tryptophan} + H_2O \quad (2)$$

$\alpha\beta$ reaction

$$\text{L-serine} + \text{indole 3-glycerol phosphate} \rightarrow \text{L-tryptophan} + \text{D-glyceraldehyde 3-phosphate} + H_2O \quad (3)$$

The activities of the α and β reactions are amplified by 1−2 orders of magnitude, when the subunits are associated to form the $\alpha_2\beta_2$ complex (*8*). Furthermore, the active sites of the α and β subunits influence each other depending on the bound substrate(s), ligand(s), or monovalent cations (*13*−*17*). Studies of the enzymatic mechanism and allosteric regulation using a spectroscopic technique and kinetic analysis suggest that the protein−ligand interaction switches the protein conformation between the low active and high active states (*18*−*21*).

[†] This study was supported in part by the National Project for Protein Structural and Functional Analysis funded by the Ministry of Education, Culture, Sports, Science, and Technology of Japan.

[‡] Coordinates have been deposited in the Protein Data Bank under file name 1WDW.

* Address correspondence to this author. Tel: 81-791-58-2937. Fax: 81-791-58-2917. E-mail: yutani@spring8.or.jp.

[§] Osaka University.

[||] Tokyo University Marine Science and Technology.

[⊥] Kumamoto University.

[#] RIKEN Harima Institute.

10.1021/bi050317h CCC: $30.25
Published on Web 08/04/2005

The first crystal structure of the tryptophan synthase $\alpha_2\beta_2$ complex from *Salmonella typhimurium* (*St*$\alpha_2\beta_2$)[1] has revealed that a 25 Å long hydrophobic tunnel connects the active sites of the α and the β subunits, through which an indole is transferred from the α to the β active sites (*22*). The crystal structures of the *St*$\alpha_2\beta_2$-bound cations or ligands for the α and β subunits have provided direct evidence for these ligand-mediated conformational changes in both subunits and have revealed that conformational changes are transmitted through the α and β subunit interface by a number of interactions, including an interaction between loop 2 of the α subunit and helix 6 of the β subunit (*23*−*30*).

However, it is still unknown how much of the conformational change in the α and/or β subunits is induced due to the $\alpha_2\beta_2$ complex formation, because the crystal structures of the isolated subunits from *S. typhimurium* have not been determined. Elucidating the conformational change in the subunits due to complex formation is indispensable for understanding the mutual activation mechanism of tryptophan synthase. Therefore, we have tried determining the X-ray crystal structures of the α, β_2, and $\alpha_2\beta_2$ complex of tryptophan synthase from a hyperthermophile, *Pyrococcus furiosus*. The tetrameric form ($\alpha_2\beta_2$) from *P. furiosus* is isolated in the α monomer and β_2 dimer in solution (*31*). In 2001, the structure of the α subunit monomer of tryptophan synthase from *P. furiosus* was determined by X-ray analysis (*32*), and recently, the X-ray crystal structure of the β_2 subunit dimer has been determined (*33*). These structures were the first three-dimensional structures of the uncomplexed tryptophan synthase α and β subunits. If the crystal structure of the $\alpha_2\beta_2$ complex of tryptophan synthase from *P. furiosus* is determined, these structures should make it possible for the first time to observe changes in the structures that occur upon the association of the individual tryptophan synthase subunits.

In this paper, we describe the X-ray crystal structure of the $\alpha_2\beta_2$ complex from *P. furiosus*. We analyzed in detail the conformational changes in each subunit upon forming the $\alpha_2\beta_2$ complex and will discuss the structural basis stabilizing the oligomeric protein from the hyperthermophile and construction of the structural architecture with activation of the catalytic function in tryptophan synthase.

EXPERIMENTAL PROCEDURES

Purification of $\alpha_2\beta_2$ from P. furiosus. The $\alpha_2\beta_2$ complex (*Pf*$\alpha_2\beta_2$) from *P. furiosus* was expressed in the *Escherichia coli* strains JM109/p$\beta\alpha$OV8 and purified as described (*31*). The protein concentration was estimated from the absorbance of the protein solution at pH 7.0 using a cell with a light path length of 1 cm. The value of $OD^{1\%}_{1cm}$ at 278.5 nm was 9.94 for *Pf*$\alpha_2\beta_2$ (*31*).

Table 1: Data Collection and Refinement Statistics of the Tryptophan Synthase $\alpha_2\beta_2$ Complex from *P. furiosus*

Characteristics of the Crystals	
space group	$P2_12_12_1$
cell parameters	
a (Å)	89.1
b (Å)	220.3
c (Å)	292.6
V_m (Å^3 D$_a^{-1}$)	2.9
solvent content (%)	58
Data Collection	
resolution (Å)	200−3.0 (3.16−3.0)
no. of unique reflections	115486
average redundancy	5.8
$I/\sigma(I)$	6.10 (1.7)
R_{merge} (%)[a,b]	9.1 (36.7)
completeness (%)[a]	99.6 (99.8)
Refinement Statistics	
resolution (Å)	40.0−3.0
no. of reflections	113449
R_{factor} (%)[c]	19.7
R_{free} (%)[d]	23.1
RMS deviations	
RMSD lengths (Å)	0.0076
RMSD angles (deg)	1.284

[a] Values within parentheses are for the last shell of data. [b] $R_{merge} = \sum_h\sum_i|(I_h - I_{hi})|/\sum_h\sum_i I_{hi} \times 100$. [c] $R_{factor} = \sum||F_o| - |F_c||/\sum|F_o| \times 100$. [d] $R_{free} = \sum||F_o| - |F_c||/\sum|F_o| \times 100$, where $|F_o|$ are test set amplitudes (5%) not used in refinement.

Enzymatic Activity Assay. The activity of the α reaction was followed by the increase in absorbance at 340 nm of NADH produced in the reactions coupled with D-glyceraldehyde 3-phosphate dehydrogenase from *Bacillus stearothermophilus* (Sigma) at pH 7.0 (*34*). The β reaction was spectrophotometrically followed by measuring the increase in absorbance at 290 nm due to the conversion of indole to L-Trp at pH 8.0 (*35*).

Crystallization and Structure Determination. Crystals of the *Pf*$\alpha_2\beta_2$ were grown by the hanging drop vapor diffusion technique. The *Pf*$\alpha_2\beta_2$ was concentrated to a final concentration of 3.6 mg mL^{-1} in 50 mM Bicine buffer (pH 7.8) containing 10 mM EDTA, 1 mM DTE, and 20 μM PLP. The precipitant reservoir solution contained 100 mM sodium citrate buffer (pH 5.6) with 8−10% PEG 8000, 60−140 mM potassium acetate, and 10% ethylene glycol. Two microliters of the precipitant buffer was mixed with an equal volume of protein solution. Crystals shaped like plates appeared at 15 °C within 1 week and grew to a maximum plate size of 0.6 × 0.4 × 0.1 mm after 4 weeks.

The diffraction experiments were done on beam line BL44XU at SPring-8 designed for biological macromolecular assemblies. The intensity data were acquired under cryogenic conditions (100 K) using a PX210 CCD camera of 210 mm by 210 mm size. For the cryogenic diffraction experiment, ethylene glycol was added to the crystallization buffer at a concentration of 25%. The diffraction data were indexed, merged, and scaled by d*TREK (*36*). The crystal belonged to the orthorhombic space group of $P2_12_12_1$ with unit cell dimensions of $a = 89.1$ Å, $b = 220.3$ Å, and $c = 292.6$ Å. This crystal diffracted to a maximum of 3.0 Å and was suitable for the structure determination (Table 1).

A structure solution using the molecular replacement method was carried out with the model molecule *Pf*$\alpha_2\beta_2$,

[1] Abbreviations: *Pf*TSase, tryptophan synthase from *Pyrococcus furiosus*; *Pf*α, tryptophan synthase α subunit from *P. furiosus*; *Pf*β_2, tryptophan synthase β_2 subunit dimer from *P. furiosus*; *Pf*β, tryptophan synthase β subunit monomer from *P. furiosus*; *Pf*$\alpha_2\beta_2$, tryptophan synthase $\alpha_2\beta_2$ complex from *P. furiosus*; *St*TSase, tryptophan synthase from *Salmonella typhimurium*; *St*α, tryptophan synthase α subunit from *S. typhimurium*; *St*β_2, tryptophan synthase β_2 subunit dimer from *S. typhimurium*; *St*β, tryptophan synthase β subunit monomer from *S. typhimurium*; *St*$\alpha_2\beta_2$, tryptophan synthase $\alpha_2\beta_2$ complex from *S. typhimurium*; *Ec*TSase, tryptophan synthase from *Escherichia coli*; *Ec*α, tryptophan synthase α subunit from *E. coli*; *Ec*$\alpha_2\beta_2$, tryptophan synthase $\alpha_2\beta_2$ complex from *E. coli*; PLP, pyridoxal 5′-phosphate; IGP, indole 3-glycerol phosphate; IPP, indole propanol phosphate; RMSD, root mean square deviation; ASA, accessible surface area.

which was constructed from the *Pf*α monomer [PDB code 1GEQ (*32*)]and *Pfβ*$_2$ dimer [PDB code 1V8Z (*33*)] models referring to the *S. typhimurium* tryptophan synthase α$_2$β$_2$ complex (*St*α$_2$β$_2$). For molecular replacement, the program EPMR was used (*37*). All refinements were executed with the CNS package (*38*). Five percent of the data was excluded during all stages of the refinements for the R_{free} calculation. After rigid-body refinement, the *R* factor of the molecular replacement solution was reduced to 26.6% (R_{free} 29.0%). Because an asymmetric unit contained three molecules of the *Pf*α$_2$β$_2$ complexes, six copies of each of the α and β molecules were analyzed using NCS (noncrystallographic symmetry) related averaging. Positional refinement using the conjugate gradient minimization, Cartesian slow cooling, and torsion angle simulated annealing with strong noncrystallographic symmetry (NCS) constraints, altered by local rebuilding, produced a final model for the three molecules of the *Pf*α$_2$β$_2$ complex in the asymmetric unit in which the *R* factor was reduced to 19.7% (R_{free} 23.1%) (Table 1). Although the resolution of the data was 3.0 Å, the electron density showed a very clear conformational arrangement favoring NCS averaging of six molecules of the α and β subunits. Three residues of loop 6 in the α subunit, which cannot be traced in the structure of the *Pf*α monomer (*32*), were visible in chain E. In the final model, three C-terminal residues in six molecules of the α subunits and the loop 6 residues in five molecules of α subunits were excluded. An average RMSD value of the corresponding C$_\alpha$ atoms among the six α and six β subunits in the crystallographic asymmetric unit was 0.024 (0.023−0.025) Å and 0.077 (0.067−0.084) Å, respectively, in the case of the α subunit residues; 167−173 were excluded in the calculation. All structural information for the *Pf*αβ pair was calculated using chain E for the α subunit and chain F for the β subunit. No residues were in the disallowed region in the Ramachandran plot (*39*). Coordinate superposition was done by the LSQKAB program (*40*). Figures showing the structures of the proteins were prepared using the MOLSCRIPT (*41*) and Raster3D programs (*42*).

RESULTS

Stimulation of α *and* β *Activities upon Formation of Pf*α$_2$β$_2$. The α activity of *Pf*α in the presence of a 4 molar excess of *Pfβ* increased with increasing temperature up to 80 °C at pH 7.0. The β activity of *Pfβ*$_2$ in the presence of a 4 molar excess of *Pf*α showed a maximum value at 95 °C at pH 8.0 (*33*). Typical stimulation patterns for the *Pfβ*$_2$ activity are demonstrated in Figure 1. The α activities were also stimulated by the addition of an excess partner subunit. The amplification of the activities by the addition of partner subunits was 3−33 times for the α activity between 40 and 80 °C and 15−43 times for the β activity between 25 and 90 °C. This indicates that the enzymatic activity of each subunit in the *Pf*TSase is activated in the presence of the partner subunit as well as in the mesophilic bacterial tryptophan synthase as already reported (*8*).

*Overall Structure of Pf*α$_2$β$_2$. The quaternary structure (PDB code 1WDW) of the *Pf*α$_2$β$_2$ complex (1272 residues, M_w of 140 kDa) was an extended linear αββα subunit arrangement as is that of *St*α$_2$β$_2$ (*22*) (Figure 2A). The *Pf*α (248 residues) in *Pf*α$_2$β$_2$ adopted a TIM barrel fold, containing two extra helices, helix 2′ and helix 8′, resulting in a total of 10 helices

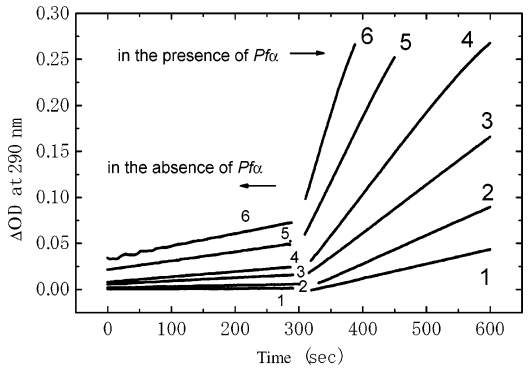

FIGURE 1: Progressive curves of the β reaction for *Pfβ*$_2$ at pH 8.0. The β reaction was monitored by the increase in the absorbance at 290 nm due to the conversion of indole to L-Trp. First, the activities were measured in the absence of *Pf*α, and after about 300 s, a 4.9-fold molar excess of *Pf*α was added to the reaction medium. Numbers 1−6 were measured at temperatures of 40, 50, 60, 70, 80, and 90 °C. The concentrations of *Pfβ*$_2$ were 15−25 μg/1.0 mL of reaction mixture.

(Figure 3A). The structure of the *Pfβ* monomer (388 residues) in the *Pf*α$_2$β$_2$ consisted of two domains, the N (residues 1−46, 81−200) and C (residues 47−80, 201−388) domains (Figures 2A and 4A). The folding patterns of *Pf*α and *Pfβ* in the *Pf*α$_2$β$_2$ complex were the same as those of the separate *Pf*α (*32*) and *Pfβ*$_2$ (*33*). The Glu36 and Asp47 of *Pf*α and Lys82 bound to PLP in *Pfβ* corresponded to the active site residues, Glu49 and Asp60, of the *St*α and Lys87 of the *Stβ*, respectively, judging from the sequences and secondary structure alignments between the subunits of the two sources (*32*, *33*). In the αβ pair of the *Pf*α$_2$β$_2$ complex, a tunnel for transferring the product of the α reaction, indole, was also observed as is in that of the *St*α$_2$β$_2$ (*22*) (Figure 2A). The tunnel passes between the N and C domains in the β subunit and connects the active sites of the α (αGlu36 and αAsp47) and β subunits (PLP cofactor colored in red in Figure 2A). The structure of an αβ pair in the complex was compared with those of both the uncomplexed *Pf*α monomer (*32*) and *Pfβ*$_2$ dimer (*33*) (Figure 2B). The average RMSD value of the C$_\alpha$ atoms between the α subunit of *Pf*α$_2$β$_2$ and the *Pf*α monomer was 0.74 Å, and that between the β subunit of *Pf*α$_2$β$_2$ and the *Pfβ*$_2$ dimer was 0.97 Å. As shown in Figure 2C, the significantly changed regions between the structures of the complex and isolated subunits were concentrated around the interface between the α and β subunits, the COMM domain (*23*, *27*) in the N domain of the β subunit, and the residues composing the tunnel wall in the β subunit.

Conformational Changes in the α *Subunit Due to Complex Formation with the* β$_2$ *Subunit.* All residues in the α subunit (chain E in PDB code 1WDW) were traceable in the crystal structure of the *Pf*α$_2$β$_2$ complex, although three residues (αG170, αA171, and αR172) in loop 6 are missing in that of the *Pf*α monomer (*32*), indicating that the α subunit in the complex becomes less mobile than the subunit alone. The RMSD values of the C$_\alpha$ atoms between the α subunit of the *Pf*α$_2$β$_2$ and the *Pf*α monomer are plotted versus the residues except for residues 170−172, which are missing in the structure of the *Pf*α monomer (Figure 3A). Three large peaks of RMSD over 2 Å were found around residues αA46, αF120, and αL165, which are located in the interface with the β subunit (Figure 2C). Residue αA46 in loop 2 (residues

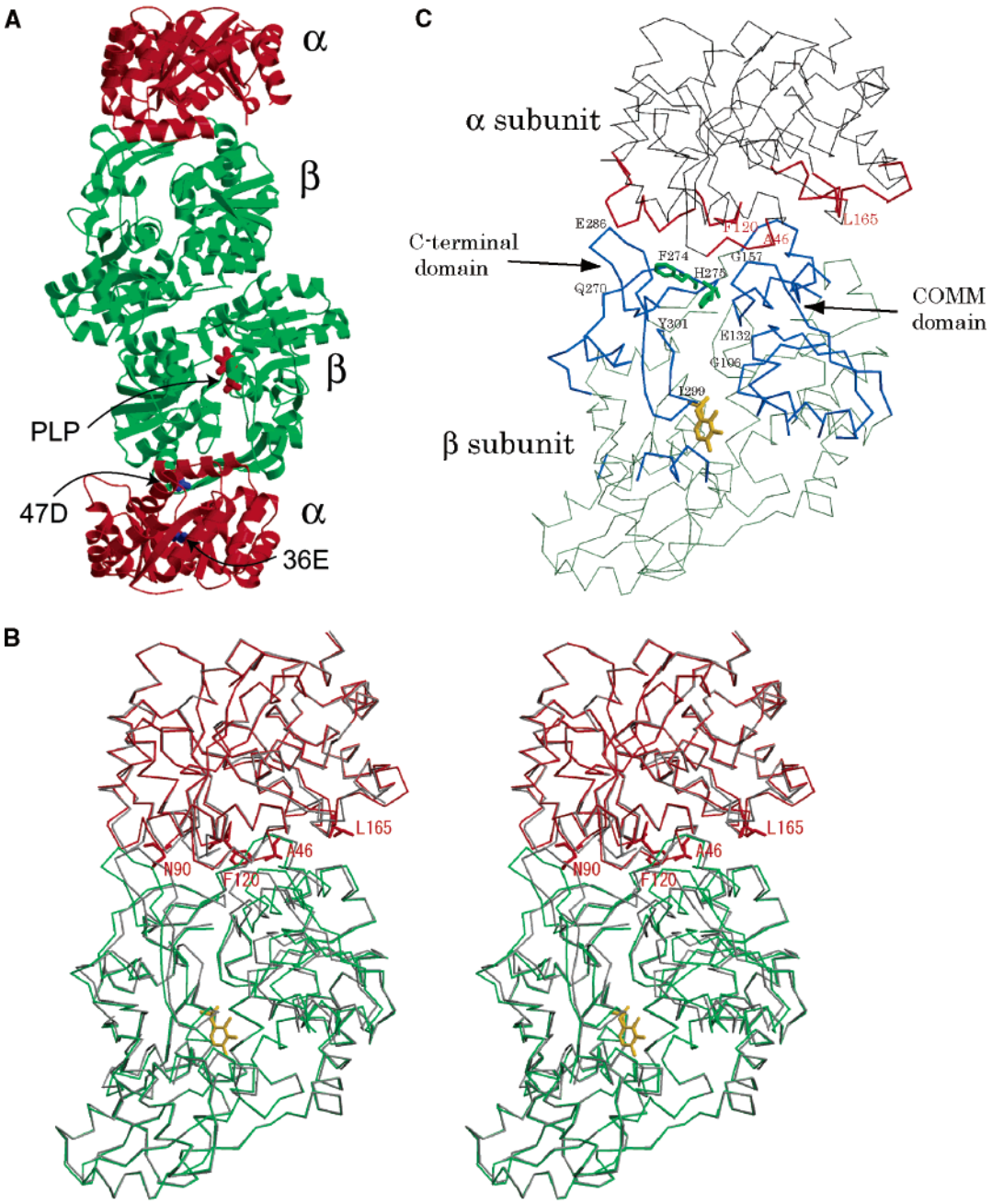

FIGURE 2: Schematic views of the crystal structure of the tryptophan synthase $\alpha_2\beta_2$ complex from *P. furiosus*. (A) Quaternary structure of $\alpha\beta\beta\alpha$. The α and β subunits are separated by color. Two α subunits (red) are located at opposite ends of the β_2 dimer (green). Each β subunit contains two domains, the N- and C-terminal domains (Figure 4A). In each α/β pair, the indole tunnel extends from the α subunit active site (Glu36 and Asp47 colored in blue) to the β subunit active site [Lys82 and coenzyme, pyridoxal phosphate (PLP), colored in red in the C-terminal domain] through the center of the interface between the N and C domains in the β subunit. (B) Schematic stereoview of an α/β pair of the *Pf*$\alpha_2\beta_2$ complex. The structures of the *Pf*α monomer and *Pf*β_2 dimer are superimposed on the *Pf*$\alpha_2\beta_2$ complex structure using C_α atoms. The *Pf*$\alpha_2\beta_2$ structure is colored in red with the α subunit and in green with the β subunit, respectively, and *Pf*α alone and *Pf*β alone are in gray. The PLP molecule is represented as a stick model colored gold. The significantly moved residues in the α subunit (Figure 3A) are depicted by residue numbers. (C) The region significantly changed in the structure of *Pf*$\alpha_2\beta_2$ compared with the structures of the subunits alone. The red line shows the α subunit residues which moved over 0.6 Å, and the blue lines show the β subunit residues which moved over 0.6 Å due to complex formation. The gold model indicates PLP, and the bold green residues show βF274 and βH275 in the β subunit. The significantly moved residues (Figures 3A and 4A) are depicted by residue numbers.

39−48) is located near the active sites of αE36 and αD47, although the RMSD values of these active site residues were small. As depicted by the arrow in Figure 3B, the αA46 residue in the complex moved toward the interface with the β subunit compared with the *Pf*α monomer. The αL165 residue in loop 6 (residues 164−176) also showed a large motion. The C_α and C_δ atoms of αL165 moved by about 4 and 9.8 Å, respectively, (gold dotted line in Figure 3B), and the side chain rotated around the $C_\alpha-C_\beta$ bond by about 150°. The motion of residues αA46 and αL165 due to complex formation, involved in the respective loop 2 and loop 6, changed the entrance into the active site (αE36) to a more open conformation thus favoring entry of the substrate, indole 3-glycerol phosphate (eq 1) (Figure 3B). Figure 5A(1) depicts the IGP modeled inside the α active site. IGP is observed to be more accessible to the solvent in the *Pf*$\alpha_2\beta_2$ complex than

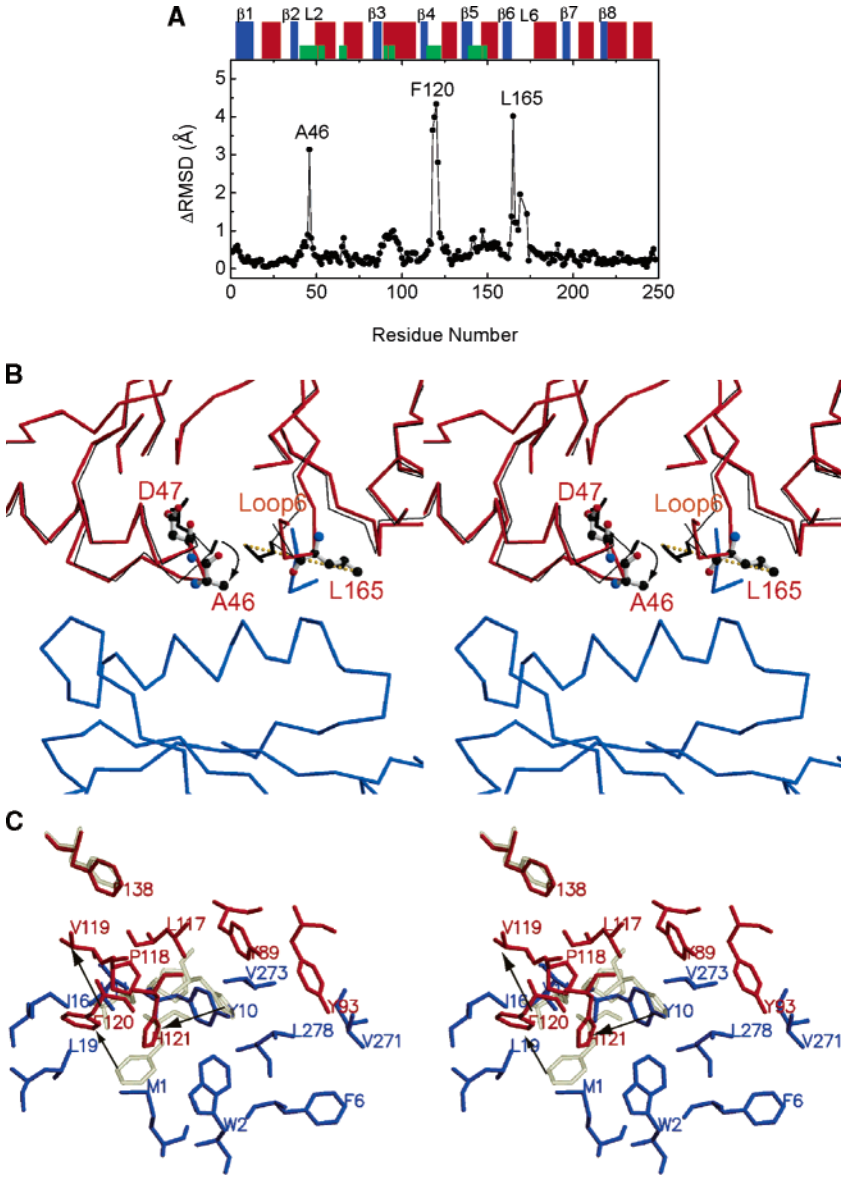

FIGURE 3: Conformational changes in the tryptophan synthase α subunit from *P. furiosus* due to complex formation. (A) The distances of the corresponding C_α atoms (RMSD) between the α subunit of *Pf*α$_2\beta_2$ and *Pf*α monomer are plotted. Red or blue blocks at the top of the figure represent the α-helix or *β*-strand for each residue number, respectively. The number of *β*-strands from *β*1 to *β*8 is the alias of the secondary structure segments of *St*α denoted by Hyde et al. (*22*). L2 and L6 represent the loops between *β*-strand 2 and α-helix 2′ and between *β*-strand 6 and α-helix 6, respectively. The green blocks represent the contact residues with the *β* subunit. (B) A stereoview of the conformational changes in the side chains of αA46 and αL165 of the α subunit upon complex formation. The red and blue chains represent the α and *β* subunits in *Pf*α$_2\beta_2$, respectively. The thin black line in the α subunit is the structure of the *Pf*α monomer. The residues of αL165 of the *Pf*α monomer and of the complex are depicted by the black lines and by the atom model colors (black balls for carbon, red ball for oxygen, and blue ball for nitrogen), respectively. Also, residues αA46 and αD47 of *Pf*α alone and of the complex are depicted by the black lines and by the atom model color, respectively. The yellow dotted line represents the movement (9.8 Å) of the C_δ atom of αL165 due to complex formation. The arrow represents the direction of movement of αA46 due to formation of the complex. (C) A stereoview of the conformational change around residue αF120 of the α subunit. The red and blue residues represent the α and *β* subunits in *Pf*α$_2\beta_2$, respectively. Three residues of αV119, αF120, and αH121 colored in gray are those of the *Pf*α monomer, and the arrowed lines show the motion of the three residues due to complex formation.

in the *Pf*α monomer [Figure 5A(2)]; that is, the entrance of a substrate at the active site of the α subunit is clearly opened in the complex form, in contrast to the entrance of the *Pf*α monomer. The αT169 residue involved in loop 6 was also significantly moved by 1.96 Å, corresponding to *St*αT183 in loop 6, which becomes visible by ligand binding (IPP) and forms a hydrogen bond with *St*αAsp60 by ligand binding (IPP) (*30*). However, in *Pf*α$_2\beta_2$, αT169 in loop 6 was far from αAsp47.

The most dramatic structural change in the α subunit occurred around residue αF120 (Figure 3C), which is located in proximity to *β*L19 and *β*I16 in the *β* subunit. αP118, αV119, and αH121 on both sides of αF120 were also significantly moved and shifted toward the *β* subunit (Figure 3C). The conformational changes in residues αP118-αV119-αF120-αH121 created an extensive hydrophobic rearrangement at the subunit interface (Figure 3C). These residues contacted *β*N9, *β*K20, *β*Y2, and *β*M1 of the *β* subunit, leading to newly created hydrophobic and hydrophilic areas in the α/*β* subunit interface. On the other hand, notable conformational changes at the *β* subunit side related to this hydrophobic rearrangement were not observed.

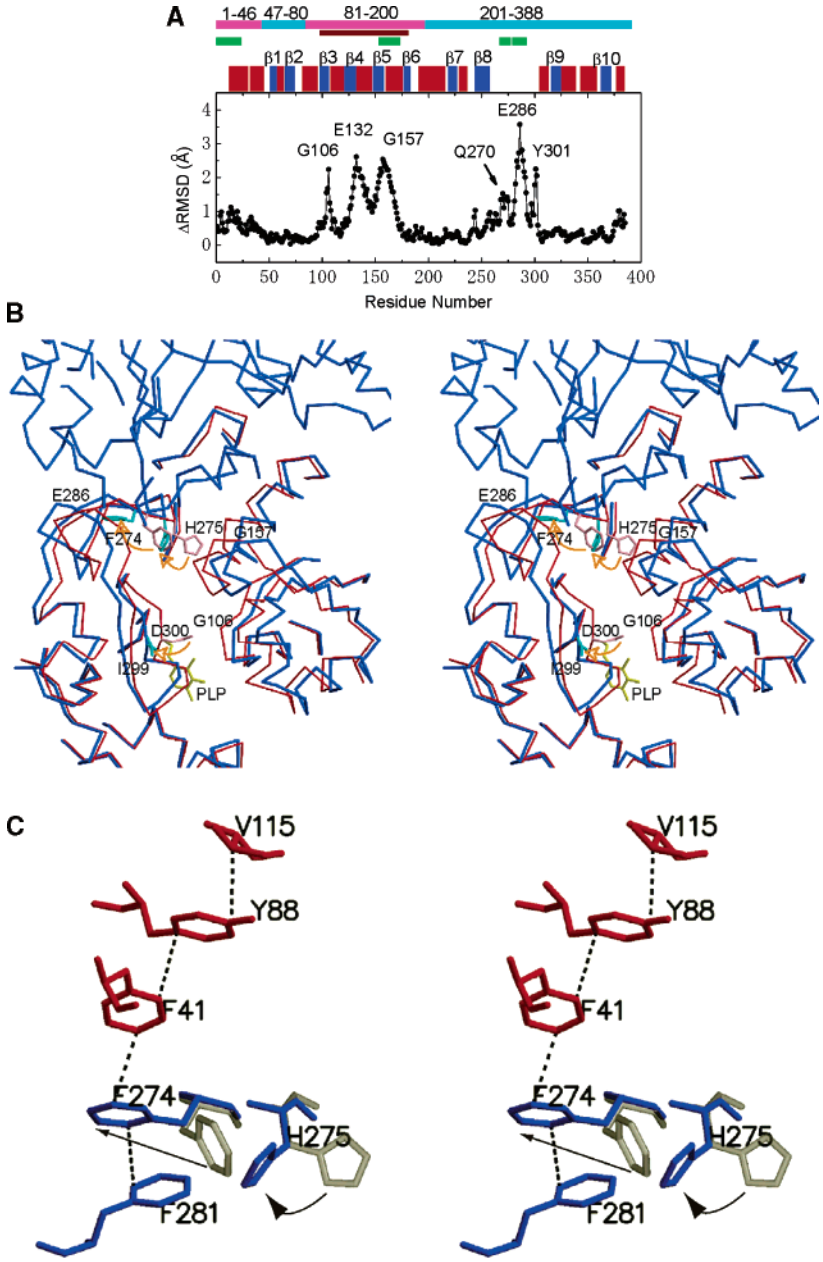

FIGURE 4: Conformational changes in the tryptophan synthase β_2 subunit from *P. furiosus* due to complex formation. (A) The distances of the corresponding C_α atoms (RMSD) between the β subunit of $Pf\alpha_2\beta_2$ and the $Pf\beta_2$ dimer are plotted. The pink and cyan blocks at the top of the figure represent the N- and C-terminal domains, respectively. The wine-colored block is the COMM domain in the N-terminal region. The green blocks represent the contact residues with the α subunit within 3.5 Å. The red or blue blocks represent the α-helix or β-strand for each residue number, respectively. The number of β-strands from β1 to β10 is the alias of the secondary structure segments of the *St*β denoted by Hyde et al. (*22*). (B) A stereoview of the indole tunnel in the β subunit from *P. furiosus*. The blue and red lines indicate the $Pf\alpha_2\beta_2$ and $Pf\beta_2$ dimer, respectively. As can be seen, the distances between the C_α atoms of βE286 and βG157 and between those of βI299 and βG106 expanded by 5.5 and 2.5 Å, respectively, due to complex formation. The side chain of βD300 was rotated to open the roof of the tunnel and to permit entrance of a substrate. The arrows in yellow represent the motions for βF274, βH275, and βD300 upon forming the complex. Residues βF274 and βH275 are explained in panel C. (C) A stereoview of the dramatic conformational changes in residues βF274 and βH275, which are called the molecular gate of the indole tunnel in *S. typhimurium* (*St*βY279 and *St*βF280). In the crystal structure of $Pf\alpha_2\beta_2$ (blue), residues βF274 and βH275 have a completely different conformation compared with the $Pf\beta_2$ dimer (gray). The arrowed lines show the motion of the two residues due to complex formation. The red residues come from the α subunit in $Pf\alpha_2\beta_2$, and the black dotted lines show the arrangement of hydrophobic residues in the subunit interface.

Conformational Changes in the β Subunit Due to Complex Formation with the α Subunit. All residues in the β subunit (chain F in PDB code 1WDW) were also traceable in the crystal structure of the $Pf\alpha_2\beta_2$ complex. The RMSD values between the corresponding C_α atoms in the β subunit of the $Pf\alpha_2\beta_2$ and the $Pf\beta_2$ dimer are plotted in Figure 4A. Structural changes between two different states of the β subunit occurred over a wide area of the molecule. One hundred forty out of a total of 388 residues were moved over 0.6 Å as shown by the blue line in Figure 2C, in contrast to 36 residues of the α subunit which is depicted in red in Figure 2C. The conformation in the interaction region with the α subunit significantly changed, but the conformational changes around the $\beta-\beta$ interaction sites were less (Figure 2C).

The areas showing the large movement were separated by two parts of the residues from 100 to 170 in the

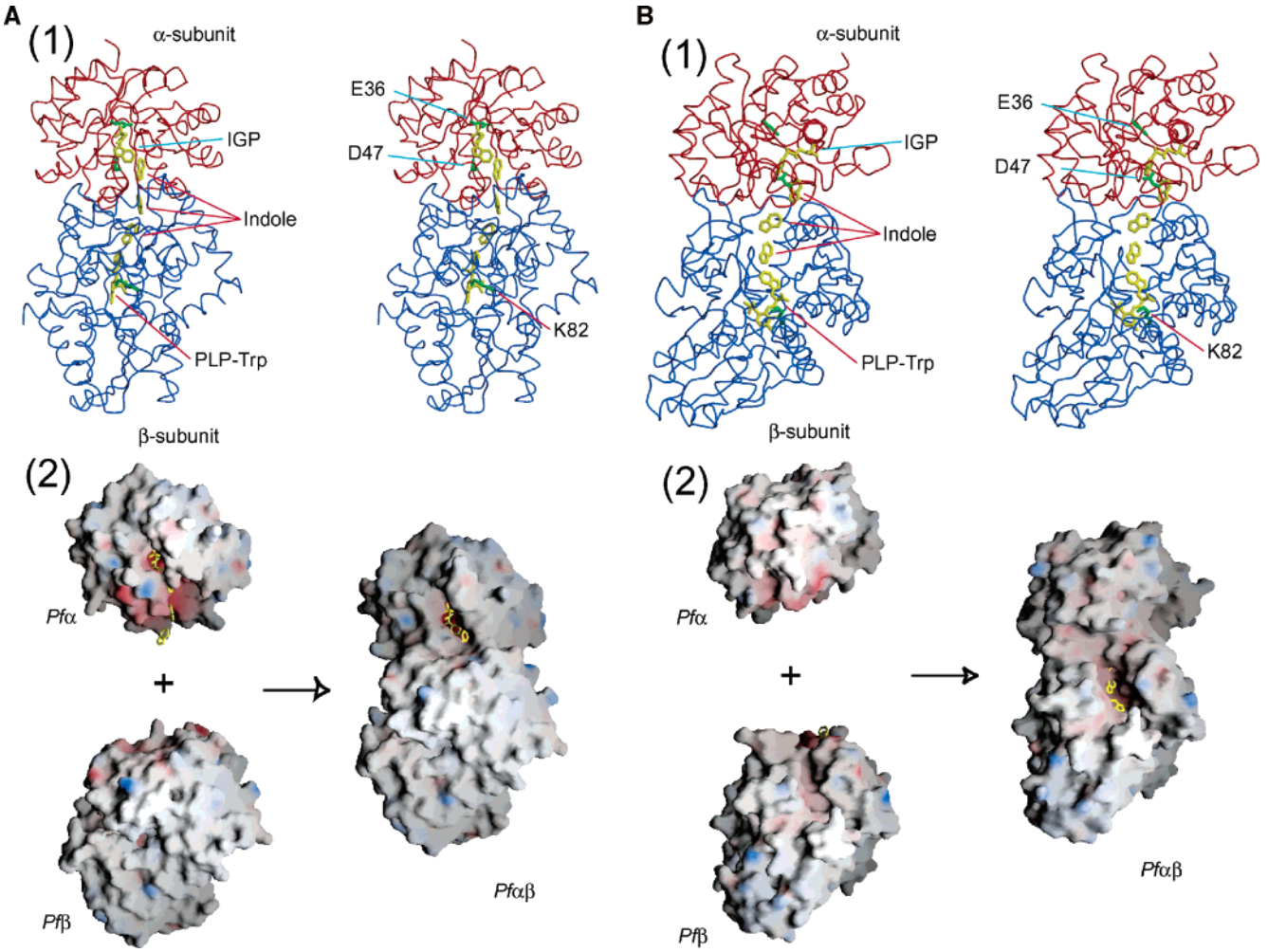

FIGURE 5: Comparison of structures of $Pf\alpha_2\beta_2$ and its subunits alone near the active sites of the α and β subunits. (A-1) and (B-1) represent the stereoviews of a backbone ribbon model of the α (red) and β (blue) subunits of $Pf\alpha_2\beta_2$ from different angles. Two catalytic residues (αE36 and αD47 colored green) and IGP (yellow) are represented in the active site of the α subunit. βK82 (green) and PLP-Trp (yellow) are displayed in the active site of the β subunit (*24*). Four indole molecules (yellow) can be modeled inside the tunnel (*22*). (A-2) and (B-2) represent the electrostatic surface potential models of the uncomplexed *Pf*α, the uncomplexed *Pf*β, and the *Pf*αβ complex from the same direction as the structures in (A-1) and (B-1), respectively. IGP is more clearly observed in the complex form (panel A-2) than in the *Pf*α monomer. Indole and PLP-Trp are clearly observed in the complex form (panel B-2) but have completely disappeared in the uncomplexed *Pf*β (panel B-2). The program GRASP was used to determine the electrostatic surface potentials (*49*). In (A-2) and (B-2), red, blue, and white represent negative, positive, and uncharged residues, respectively.

N-terminal domain and residues from 255 to 303 in the C-terminal domain (Figures 2C and 4A). The moved N-terminal domain in the β subunit corresponds to the mobile (*23*) or communication (COMM) domain (from β-strand 3 to β-strand 6) (*27*) in the structure of $St\alpha_2\beta_2$. The COMM domain, which is involved in the conformational changes upon binding of the substrate ligands and on one side interacts with the α subunit via loop αL2 and on the other side with the β active site, has been reported to play an important role in the allosteric communication between the α and β active sites (*23*, *27*, *28*). When the average RMSD values of the C_α atoms between the β subunits of $Pf\alpha_2\beta_2$ and the $Pf\beta_2$ dimer were calculated for only the mobile parts of the COMM (71 residues) and C-terminal (49 residues) domains, they were 0.27 Å for the COMM domain and 0.61 Å for the C-terminal domain. The slight value of the COMM domain and the bigger one of the C-terminal domain suggest that the COMM domain of the β subunit moves as a rigid body when the α and β_2 subunits associate, but the C-terminal domain moves in an induced-fit conformational change. After both β subunits of the complex and the dimer were superimposed using all of the C_α atoms except for those of the COMM domain, the relation of both COMM domains was examined and resulted in the fact that the COMM domain in the β_2 dimer was rotated 6.87° about an axis and then translated 1.74 Å between the centroids of the two domains due to complex formation. When the $St\alpha_2\beta_2$ binds ligands in the α active site, the conformational changes have been reported to be transmitted to the β active site by a remarkable rigid-body movement of the COMM domain (*28*). These results suggest that the rigid-body movement is an important aspect of the transmission of information, such as ligand bindings or complex formation.

Among residues showing a significant movement, three residues, βG157, βQ270, and βE286 in Figure 4A, are located in loops near the interface of the α and β subunits (Figure 2C). The other three residues, βG106, βE132, and βY301, constitute parts (wall) of the indole tunnel. The large movements expanded the width of the inner side of the indole tunnel enclosed by the N- and C-terminal domains (Figures 2C and 4B). For example, the distances between the C_α atoms of βE286 and βG157, which are located at the interaction

site with the α subunit, were 21.7 and 16.2 Å for the complex structure and for the β_2 subunit dimer, respectively, (Figure 4B), indicating that the distance between the two residues expanded by 5.5 Å due to complex formation. Furthermore, the distances between βI299 and βG106, which are located near PLP and are assumed to be the exit of the tunnel, were 11.76 and 9.28 Å, in the structures of the complex and of the β_2 subunit dimer, respectively.

Dramatic conformational changes were found in residues βF274 and βH275 (Figures 2C and 4B,C), which correspond to residues *St*βY279 and *St*βF280 postulated to be the molecular gate into the indole tunnel (*23*). In the crystal structure of *Pf*$\alpha_2\beta_2$, the side chains of residues βF274 and βH275 were in a completely different arrangement (colored blue in Figure 4C) compared to those of the *Pf*β_2 dimer (gray in Figure 4C). Both side chains of βF274 and βH275 in the complex rotated with a side chain dihedral angle by 125° and 100°, respectively, compared with the position in the *Pf*β_2 dimer, and the gate of the indole tunnel opened as clearly observed in Figure 4B. In the crystal structure, all six β subunits (chains B, C, F, G, J, and K) in the asymmetric unit showed an open conformation at the gate. The main chains of the residues near these two residues also moved to broaden the indole tunnel due to complex formation. As shown in Figure 4B, the side chain of βD300, which is located near PLP and covers the roof of the tunnel in the *Pf*β_2 dimer, was rotated to open the roof and to permit entry of a substrate, L-Ser, upon complex formation (eq 2). Figure 5B demonstrates that the indole and PLP-Trp modeled inside of the tunnel of the *Pf*$\alpha_2\beta_2$ complex are accessible to the solvent; that is, the entrance of a substrate at the active site of the β subunit is clearly opened in the complex form, although the entrance of the *Pf*β_2 dimer is completely closed [Figure 5B(2)]. These results indicate that the indole tunnel in the β subunit converted to a shape with a broader tunnel and a big entrance at the active site of the β subunit due to the formation of the *Pf*$\alpha_2\beta_2$ complex.

Moreover, the rotation in the side chains of βF274 and βH275 created an extremely long hydrophobic network through the α and β subunits (βF281-βF274-αF41-αY88-αV115) (Figure 4C). The movement of these two residues could connect the α and β subunits through consecutive hydrophobic residues, resulting in a strong binding of *Pf*α with *Pf*β and stabilization of the $\alpha_2\beta_2$ complex structure (Figure 4C).

Differences in β−β Subunit Interaction between Pf$\alpha_2\beta_2$ *and the Pf*β_2 *Dimer.* The conformation of the *Pf*$\alpha_2\beta_2$ complex at the β−β subunit interface was the same as that of the *Pf*β_2 dimer. The stability of the dimer form (*Pf*β_2) does not change in *Pf*β_2 alone and in the complex form (*31*). *Pf*β_2 does not dissociate in the pH region above 6, but dissociates into a monomer in the acidic region, resulting in a remarkable decrease in the stability (*31*, *33*). These reported results are in accord with the present finding that the β−β subunit interaction site hardly changes upon complex formation. The β−β subunit interaction is very strong and is important for the stabilization of *Pf*β_2.

Conformational Changes in Residues around the Active Sites Due to Complex Formation. The essential catalytic residue αE36 (Figure 2A) in the *Pf*$\alpha_2\beta_2$ complex for the first step of the α reaction, which interacts with the hydroxyl group at C3′ of the substrate (IGP) (*26*), was positioned in similar geometry to that of the *Pf*α monomer. The geometry of *Pf*αY161 corresponding to *St*αY175, which is another binding residue of IGP (*26*), was also identical in the two different states. Residues (αM86, αL113, αV115, αG115, αF153, αL139, and αV218) that compose the inner wall of the α subunit tunnel near αE36 did not change as compared with those in the isolated α subunit. In the case of αD47, which is the essential catalytic residue for the second step of the α reaction and located in the α and β subunit interface (Figure 2A), the side chains of αD47 in the complex form only slightly shifted toward the β subunit compared to those of the isolated α subunit. The preceding residue, αA46, significantly shifted toward the interface with the β subunit due to complex formation as shown in Figure 3B. These results indicate that the $\alpha_2\beta_2$ complex formation did not introduce a geometric strain which might facilitate better catalysis but resulted in a more open conformation favoring the entry of the substrate at the active site together with the remarkable shifts of αL165. This suggests that substrates easily reach the active site. For *Pf*$\alpha_2\beta_2$, better structural changes for the stimulation of activities upon the binding of ligands might be expected, because the binding of substrates or ligands triggers the conformational changes favoring allosteric communication in *St*$\alpha_2\beta_2$ (*24*−*30*).

The βK82 forming a Schiff base with PLP had almost similar geometries in the two structures. All of the changes in the *Pf*β subunit due to complex formation opened an entrance at the β active site and also widened the indole tunnel as previously mentioned.

DISCUSSION

Stabilization Arising from Interactions between α *and* β *Subunits in the Tryptophan Synthase* $\alpha_2\beta_2$ *Complex.* The factors stabilizing the *Pf*α monomer (*32*) and *P*β_2 dimer (*33*) from the structural features of the two separated subunits have been reported compared with the structures for both subunits in *St*$\alpha_2\beta_2$. In this study, we can clarify the features of the newly generated interaction at the interface between the α and β subunits of *Pf*$\alpha_2\beta_2$ in comparison with the interaction at the subunit interface of *St*$\alpha_2\beta_2$, and the contribution of these interactions to the stability of the *Pf*$\alpha_2\beta_2$ complex.

Hydrogen bonds and ion pairs (salt bridges) at the interface between the α and β subunits were examined, except for water-mediated hydrogen bonds. The number of hydrogen bonds within a 3.6 Å distance was 30 per α/β pair in *Pf*$\alpha_2\beta_2$ and 25 in *St*$\alpha_2\beta_2$ (PDB code 1BKS). The number of ion pairs (13 within 5 Å) in the subunit interface of *Pf*$\alpha_2\beta_2$ was greater by 11 than that (only 2) in *St*$\alpha_2\beta_2$ (Table 2). The increases in the number of hydrogen bonds and ion pairs in *Pf*$\alpha_2\beta_2$ compared to *St*$\alpha_2\beta_2$ might contribute to the stabilization of the *Pf*$\alpha_2\beta_2$ complex.

The movements of residues due to complex formation of *Pf*$\alpha_2\beta_2$ induced a rearrangement of the consecutive hydrophobic residues in the interface of the α and β subunits (Figures 3C and 4C). We examined the contribution to stabilization of the *Pf*$\alpha_2\beta_2$ complex due to the hydrophobic interaction occurring in the α/β subunit interface. The Gibbs energy change (ΔG_{HP}) for stabilization originating from the hydrophobic interaction is correlated with changes in the accessible surface area (ASA) of atoms (*43*) due to complex

Table 2: Ion Pairs within 5 Å in the α/β Subunit Interface of Trptophan Synthases

proteins	donor	acceptor	distance (Å)
Pf$\alpha_2\beta_2$ complex	αArg66 NH1	βGlu286 OE1	2.8
	αArg148 NH2	βGlu17 OE1	3.1
	αArg148 NH2	βGlu13 OE1	3.3
	αLys49 NZ	βGlu167 OE2	3.7
	αLys49 NZ	βGlu167 OE1	3.8
	αArg148 NH1	βGlu17 OE1	4.0
	βHis275 ND1	αAsp43 OD1	4.4
	αArg148 NH2	βGlu13 OE2	4.6
	αArg66 NH2	βGlu286 OE1	4.6
	βLys162 NZ	αAsp43 OD1	4.7
	αArg148 NH1	βGlu13 OE1	4.8
	αArg66 NH1	βGlu286 OE2	4.8
	βHis275 ND1	αAsp43 OD2	4.8
St$\alpha_2\beta_2$ complex	βLys167 NZ	αAsp56 OD2	3.0
	βLys167 NZ	αAsp56 OD1	3.3

formation. The area (ASA value) for the interface of an α/β pair was calculated using the procedure of Connolly (*44*) with a probe radius of 1.4 Å: the area corresponds to the difference between the summation of the ASA values of each subunit structure and the ASA value of the complex structure. The ASA value per α/β pair due to complex formation was greater by 585 Å^3 in *Pf*$\alpha_2\beta_2$ than in *St*$\alpha_2\beta_2$. The differences in the ASA values due to the nonpolar (C/S) and polar (N/O) atoms were 378 and 207 Å^3, respectively. The increase ($\Delta\Delta G_{HP}$) in ΔG_{HP} per α/β pair due to the hydrophobic interaction for *Pf*$\alpha_2\beta_2$ compared to *St*$\alpha_2\beta_2$ was estimated to be 52.8 kJ mol^{-1} using the equation (*43*):

$$\Delta\Delta G_{HP}\,(\text{kJ mol}^{-1}) = 0.154\Delta\Delta\text{ASA}_{\text{nonpolar}} - 0.0254\Delta\Delta\text{ASA}_{\text{polar}}$$

These results indicate that stabilization due to complex formation of *Pf*TSase is caused not only by a hydrophilic interaction but also by a hydrophobic interaction at the subunit interface, compared with that of *St*TSase. The stabilization due to complex formation of *Pf*TSase has been experimentally reported. The denaturation temperature of 87.2 °C for the *Pf*α monomer at pH 9.4 increases to 104.6 °C in the complex form (*31*). Furthermore, the association constant between the α and β subunits has been reported to be higher by 2 orders of magnitude in *Pf*TSase than in *Ec*TSase (*31*). These results indicate that the stabilization in the subunit interface of *Pf*$\alpha_2\beta_2$ contributes to the enhanced stability of the α subunit, of which the denaturation temperature is lower in the monomer state than the growth temperature near 100 °C or more for *P. furiosus*.

Comparison with the Structures of the St$\alpha_2\beta_2$ *Complex.* The crystal structures of *St*$\alpha_2\beta_2$ with ligands bound at the α and β active sites have revealed (*23*−*30*) that the regions in which major movements occur depending on the ligand are loop αL2, loop αL6, helix βH6 included in the COMM domain, and the COMM domain, which are critical for the α and β activities and for the allosteric communication between the two subunits (*23*−*30*). In the absence of a ligand, loop αL6 for the α subunit of *St*$\alpha_2\beta_2$ is mobile for opening the entrance of a substrate (*22*). When an inhibitor, IPP, is bound at the α active site, stabilization of the loop αL2 residues and closure of loop αL6 are introduced (*28*). The ordering and mutual stabilization of loops αL6 and αL2 change the intersubunit interface, leading to an ordering and repositioning of helix βH6. In the case of binding with a natural substrate, IGP (*30*), loop αL6 is still mobile, and the side chain of the gating residue in the tunnel, βTyr279, adopts an "open channel" conformation. Because of the altered hydrogen-bonding pattern of loop αL2 in the *St*$\alpha_2\beta_2$ complex with IGP, a remarkable rigid-body movement of the COMM domain including helix βH6 results in an open β subunit in the *St*$\alpha_2\beta_2$ complex with IGP, where PLP at the β active site is accessible to the solvent (*28*).

In the case of *Pf*$\alpha_2\beta_2$, all of the residues in the structure of the α subunit can be modeled in the absence of any ligands. As shown in Figure 5A, the entrance of a substrate in the α subunit is sufficiently opened due to large movements of αA46 and αL165 (Figure 3A,B), although loop αL6 is not mobile. The number of hydrogen bonds including ion pairs between loop αL2 and the COMM domain of the β subunit was 7 and 4 in *Pf*$\alpha_2\beta_2$ and in *St*$\alpha_2\beta_2$, respectively, in the absence of ligands (PDB code 1BKS). This indicates that the stronger interaction between the α and β subunits of *Pf*$\alpha_2\beta_2$ might induce the movement of the COMM domain due to complex formation even in the absence of ligands, because it has been observed that extra newly formed hydrogen bonds between loop αL2 and the COMM domain due to the ligand bindings of *St*$\alpha_2\beta_2$ result in movement of the COMM domain (*23*, *27*). The side chains of the gate residues, βPhe274 and βHis275 of *Pf*$\alpha_2\beta_2$, to the tunnel of the β subunit are already open (Figure 4B,C), and the width of the tunnel in the β subunit becomes broad (Figures 2C and 4B). The β active site is also accessible to the solvent (Figure 5B). These structural features of *Pf*$\alpha_2\beta_2$ are similar to the structure of *St*$\alpha_2\beta_2$ bound the natural substrate, IGP, rather than the structures of the *Pf*α monomer and *Pf*β_2 dimer. The present results indicate that the α and β active sites of *Pf*$\alpha_2\beta_2$ even in the absence of a ligand are open (Figure 5), which favor the entry of substrates compared with the structures of the uncomplexed *Pf*α and *Pf*β_2. The hyperthermophile *Pf*$\alpha_2\beta_2$ structure is considerably different from that of the mesophile *St*$\alpha_2\beta_2$ in the absence of ligands. This difference might be necessary for the stabilization of the hyperthermophile protein.

Stimulation Mechanism of Enzymatic Activity Due to the $\alpha_2\beta_2$ *Complex Formation.* The α and β activities due to formation of the *Pf*$\alpha_2\beta_2$ complex were stimulated compared with those of the respective subunits alone (Figure 1). In the case of *Ec*TSase, the stimulation of activities has decreased in the mutants of *Ec*α substituted at positions which are located far from the active site. The mutations with a decrease in the association constants between the α and β subunits lead to a decrease in the stimulation of activities in the α and β reactions, indicating that the subunit association plays a crucial role in the stimulation of the activities (*45*, *46*).

Furthermore, it has been reported that the number of residues of local folding coupled to the subunit association in tryptophan synthase is less in *Pf*TSase than in *Ec*TSase based on thermodynamic analysis of the subunit association (*31*, *47*). On the basis of these results, it has been predicted that more dramatic changes occur in the three-dimensional structures of the *Ec*TSase from mesophiles, compared with conformational changes in *Pf*TSase due to complex formation (*31*). In the case of *Ec*TSase, the structure of only the α subunit has been solved in the crystal state in the immediate

past. As predicted, the helical structure corresponding to helix 2′ of the α subunit involved in *St*$\alpha_2\beta_2$ has been observed to be destroyed in the isolated *Ec*α (*48*). Although the structure of the complex form of *Ec*TSase has not been solved, it can be assumed that the structure of *Ec*$\alpha_2\beta_2$ is similar to that of *St*$\alpha_2\beta_2$ because the sequence identities of *Ec*TSase and *St*TSase are high (85% for the α subunit and 97% for the β subunit). That is, helix 2′ of the α subunit from mesophiles, which is essential for the α reaction, might be constructed by coupling to binding with the β subunit for the TSase from mesophiles.

On the other hand, helix 2′ of *Pf*α is already intact in an uncomplexed state (*32*). It can be concluded that the association mode of the α/β subunits from a hyperthermophile is different from that from mesophiles and that the α/β subunit association occurs by recognition between residues of both subunits in a "lock and key" mode in *Pf*TSase from a hyperthermophile but as an "induced fit" mode with large conformation changes in *Ec*TSase and *St*TSase from mesophiles. Therefore, the mutual activation mechanism due to complex formation of *Pf*$\alpha_2\beta_2$ from a hyperthermophile should be remarkably different from that of *St*$\alpha_2\beta_2$ from a mesophile. On the basis of many investigations on the structures and biochemical kinetics for *St*$\alpha_2\beta_2$, a key feature of the allosteric interaction between the active sites of the α and β subunits seems to be the switching of conformations between the "open low activity" and "closed high activity" states, which are triggered by the binding of ligands to the active sites, and the stimulation of the activities correlates to the structure with the closed high activity induced by ligand binding (*12*, *19*, *28*, *50*−*52*). In the case of *Pf*$\alpha_2\beta_2$, conformational changes due to complex formation, such as opening of the entrances of the active sites and the gate into the β subunit and broadening of the indole tunnel, might facilitate the binding of substrates. The binding of substrates is supposed to be the first step to induce the conformation changes with "high activity". Additional biochemical experiments and structural analyses of ligand bound proteins for hyperthermophile tryptophan synthase will reveal the difference in the mutual activation mechanism due to the $\alpha_2\beta_2$ complex formation of tryptophan synthase between mesophiles and hyperthermophiles.

CONCLUSIONS

The three-dimensional structure of the tryptophan synthase $\alpha_2\beta_2$ complex from *P. furiosus*, with the structures of the isolated α monomer and β_2 dimer, is the first structural set for comparing the conformational changes due to complex formation. All of the residues in both the α and β subunits were modeled in the crystal structure of *Pf*$\alpha_2\beta_2$. The enzymatic activity of each α or β subunit of *Pf*TSase was confirmed to be significantly activated due to complex formation in the presence of the partner subunit as well as that in the mesophilic prokaryotic bacterial proteins.

To elucidate the structural basis of the mutual activation of the tryptophan synthase $\alpha_2\beta_2$ complex, the conformational changes in *Pf*$\alpha_2\beta_2$ due to complex formation were analyzed in detail, compared with the structures of the *Pf*α monomer and *Pf*β_2 dimer and the complex form of the *St*TSase from mesophile. The major structural changes in *Pf*$\alpha_2\beta_2$ compared with the uncomplexed structures of *Pf*α and *Pf*β_2 occurred in the region essential for the function of tryptophan synthase. The main conformational changes in the α and β subunits due to complex formation were as follows: (1) Structural changes in the β subunit were greater than those in the α subunit: 140 out of a total of 388 residues of the β subunit are moved over 0.6 Å in contrast to 36 out of a total of 248 residues of the α subunit. (2) Changes in the α subunit mainly occurred at the α/β subunit interface. (3) Large movements of αA46 and αL165 in the respective loop 2 and loop 6 of the α subunit due to complex formation constructed an open conformation favoring entry of the substrate into the α active site, although the open form in the *St*$\alpha_2\beta_2$ complex is due to movable residues in loop 6 which are not traceable in the crystal structure. (4) The major changes in the β subunit were the broadening of a long tunnel through which the α subunit product (indole) is transferred to the β active site and the opening of an entrance at the β active site. The molecular gates in the tunnel from the α to β subunits were also an open form. In the case of *St*$\alpha_2\beta_2$, the gate in the tunnel is closed, and the entrance of a substrate in the β active site is also closed. (5) The conformational changes in both the α and β subunits due to complex formation contribute to stabilization of the subunit association, which is critical for stimulation of the activity. (6) The mutual activation mechanism due to complex formation of *Pf*$\alpha_2\beta_2$ from hyperthermophiles seemed to be remarkably different from that of *St*$\alpha_2\beta_2$ from the mesophile.

ACKNOWLEDGMENT

We thank Prof. Yoshiki Matsuura at Osaka University for the calculation of the rigid-body movements.

REFERENCES

1. Koshland, D. E. J. (1958) Protein structure and enzyme action, *Proc. Natl. Acad. Sci. U.S.A. 44*, 98−104.
2. Monod, J. (1966) From enzymatic adaptation to allosteric transitions, *Science 154*, 475−483.
3. Williamson, J. R. (2000) Induced fit in RNA-protein recognition, *Nat. Struct. Biol. 7*, 834−837.
4. Spolar, R. S., and Record, M. T., Jr. (1994) Coupling of local folding to site-specific binding of proteins to DNA, *Science 263*, 777−784.
5. Lee, S. J., Imamoto, N., Sakai, H., Nakagawa, A., Kose, S., Koike, M., Yamamoto, M., Kumasaka, T., Yoneda, Y., and Tsukihara, T. (2000) The adoption of a twisted structure of importin-beta is essential for the protein−protein interaction required for nuclear transport, *J. Mol. Biol. 302*, 251−264.
6. Lee, S. J., Sekimoto, T., Yamashita, E., Nagoshi, E., Nakagawa, A., Imamoto, N., Yoshimura, M., Sakai, H., Chong, K. T., Tsukihara, T., and Yoneda, Y. (2003) The structure of importin-beta bound to SREBP-2: nuclear import of a transcription factor, *Science 302*, 1571−1575.
7. Goh, C. S., Milburn, D., and Gerstein, M. (2004) Conformational changes associated with protein−protein interactions, *Curr. Opin. Struct. Biol. 14*, 104−109.
8. Miles, E. W. (1979) Tryptophan synthase: Structure, function, and subunit interaction, *Adv. Enzymol. Relat. Areas Mol. Biol. 49*, 127−186.
9. Miles, E. W. (1986) Pyridoxal phosphate enzymes catalyzing β-elimination and β-replacement reactions, in *Pyridoxal Phosphate: Chemical, Biochemical, and Medical Aspects* (Dolphin, D., Poulson, R., and Avramovic, O., Eds.) Part B, pp 253−310, John Wiley and Sons, New York.
10. Miles, E. W. (1991) Structural basis for catalysis by tryptophan synthase, *Adv. Enzymol. Relat. Areas Mol. Biol. 64*, 93−172.
11. Miles, E. W. (1995) Tryptophan synthase. Structure, function, and protein engineering, *Subcell. Biochem. 24*, 207−254.
12. Pan, P., Woehl, E., and Dunn, M. F. (1997) Protein architecture, dynamics and allostery in tryptophan synthase channeling, *Trends Biochem. Sci. 22*, 22−27.

13. Ruvinov, S. B., Ahmed, S. A., McPhie, P., and Miles, E. W. (1995) Monovalent cations partially repair a conformational defect in a mutant tryptophan synthase $\alpha_2\beta_2$ complex (β-E109A), *J. Biol. Chem. 270*, 17333−17338.
14. Peracchi, A., Mozzarelli, A., and Rossi, G. L. (1995) Monovalent cations affect dynamic and functional properties of the tryptophan synthase alpha 2 beta 2 complex, *Biochemistry 34*, 9459−9465.
15. Peracchi, A., Bettati, S., Mozzarelli, A., Rossi, G. L., Miles, E. W., and Dunn, M. F. (1996) Allosteric regulation of tryptophan synthase: effects of pH, temperature, and α-subunit ligands on the equilibrium distribution of pyridoxal 5′-phosphate-L-serine intermediates, *Biochemistry 35*, 1872−1880.
16. Fan, Y. X., McPhie, P., and Miles, E. W. (2000) Regulation of tryptophan synthase by temperature, monovalent cations, and an allosteric ligand. Evidence from Arrhenius plots, absorption spectra, and primary kinetic isotope effects, *Biochemistry 39*, 4692−4703.
17. Weber-Ban E., Hur, O., Bagwell, C., Banik, U., Yang, L. H., Miles, E. W., and Dunn, M. F. (2001) Investigation of allosteric linkages in the regulation of tryptophan synthase: the roles of salt bridges and monovalent cations probed by site-directed mutation, optical spectroscopy, and kinetics, *Biochemistry 40*, 3497−3511.
18. Fan, Y. X., McPhie, P., and Miles, E. W. (2000) Thermal repair of tryptophan synthase mutations in a regulatory intersubunit salt bridge. Evidence from Arrhenius plots, absorption spectra, and primary kinetic isotope effects, *J. Biol. Chem. 275*, 20302−20307.
19. Brzovic, P. S., Ngo, K., and Dunn, M. F. (1992) Allosteric interactions coordinate catalytic activity between successive metabolic enzymes in the tryptophan synthase bienzyme complex, *Biochemistry 31*, 3831−3839.
20. Osborne, A., Teng, Q., Miles, E. W., and Phillipps, R. S. (2003) Detection of open and closed conformations of tryptophan synthase by ^{15}N-heteronuclear single-quantum coherence nuclear magnetic resonance of bound 1-^{15}N-L-tryptophan, *J. Biol. Chem. 278*, 44083−44090.
21. Ferrari, D., Niks, D., Yang, L.-H., Miles, E. W., and Dunn, M. F. (2003) Allosteric communication in the tryptophan synthase bienzyme complex: Roles of the β-subunit aspartate 305-arginine 141 salt bridge, *Biochemistry 42*, 7807−7818.
22. Hyde, C. C., Ahmed, S. A., Padlan, E. A., Miles, E. W., and Davies, D. R. (1988) Three-dimensional structure of the tryptophan synthase $\alpha_2\beta_2$ multienzyme complex from *Salmonella typhimurium*, *J. Biol. Chem. 263*, 17857−17871.
23. Rhee, S., Parris, K. D., Ahmed, S. A., Miles, E. W., and Davies, D. R. (1996) Exchange of K^+ or Cs^+ for Na^+ induces local and long-range changes in the three-dimensional structure of the tryptophan synthase $\alpha_2\beta_2$ complex, *Biochemistry 35*, 4211−4221.
24. Rhee, S., Parris, K. D., Hyde, C. C., Ahmed, S. A., Miles, E. W., and Davies, D. R. (1997) Crystal structures of a mutant (βK87T) tryptophan synthase $\alpha_2\beta_2$ complex with ligands bound to the active sites of the α- and β-subunits reveal ligand-induced conformational changes, *Biochemistry 36*, 7664−7680.
25. Rhee, S., Miles, E. W., Mozzarelli, A., and Davies, D. R. (1998) Cryocrystallographpy and microspectrophotometry of a mutant (αD60) tryptophan synthase $\alpha_2\beta_2$ complex reveals allosteric roles of αAp60, *Biochemistry 37*, 10653−10659.
26. Rhee, S., Miles, E. W., and Davies, D. R. (1998) Cryocrystallograpy of a true substrate, indole-3-glycerol phosphate, bound to a mutant (αD60) tryptophan synthase $\alpha_2\beta_2$ reveals the correct orientation of active site αGlu49, *J. Biol. Chem. 273*, 8553−8555.
27. Schneider, T. R., Gerhardt, E., Lee, M., Liang, P. H., Anderson, K. S., and Schlichting, I. (1998) Loop closure and intersubunit communication in tryptophan synthase, *Biochemistry 37*, 5394−5406.
28. Weyand, M., and Schlichting, I. (1999) Crystal structure of wild-type tryptophan synthase complexed with the natural substrate indole-3-glycerol phosphate, *Biochemistry 38*, 16469−16480.
29. Sachpatzidis, A., Dealwis, C., Lubetsky, J. B., Liang, P. H., Anderson, K. S., and Lolis, E. (1999) Crystallographic studies of phosphonate-based α-reaction transition-state analogues complexed to tryptophan synthase, *Biochemistry 38*, 12665−12674.
30. Kulik, V., Weyand, M., Seidel, R., Niks, D., Arac, D., Dunn, M. F., and Schlichting, I. (2002) On the role of αThr183 in the allosteric regulation and catalytic mechanism of tryptophan synthase, *J. Mol. Biol. 324*, 677−690.
31. Ogasahara, K., Ishida, M., and Yutani, K. (2003) Stimulated interaction between α and β subunits of tryptophan synthase from hyperthermophile enhances its thermal stability, *J. Biol. Chem. 278*, 8922−8928.
32. Yamagata, Y., Ogasahara, K., Hioki, Y., Lee, S. J., Nakagawa, A., Nakamura, H., Ishida, M., Kuramitsu, S., and Yutani, K. (2001) Entropic stabilization of the tryptophan synthase α-subunit from a hyperthermophiles, *Pyrococcus furiosus*, *J. Biol. Chem. 276*, 11062−11071.
33. Hioki, Y., Ogasahara, K., Lee, S. J., Ma, J., Ishida, M., Yamagata, Y., Matsuura, Y., Ota, M., Ikeguchi, M., Kuramitsu, S., and Yutani, K. (2004) The crystal structure of the tryptophan synthase β_2 subunit from the hyperthermophile, *Pyrococcus furiosus*: investigation of stabilization factors, *Eur. J. Biochem. 271*, 2624−2635.
34. Creighton, T. E. (1970) A steady-state kinetic investigation of the reaction mechanism of the tryptophan synthetase of *Escherichia coli*, *Eur. J. Biochem. 13*, 1−10.
35. Miles, E. W., Bauerle, R., and Ahmed, S. A. (1987) Tryptophan synthase from *Escherichia coli* and *Salmonella typhimurium*, *Methods Enzymol. 142*, 398−414.
36. Pflugrath, J. W. (1999) The finer things in X-ray diffraction data collection, *Acta Crystallogr., Sect. D: Biol. Crystallogr. 55* (Part 10), 1718−1725.
37. Kissinger, C. R., Gehlhaar, D. K., and Fogel, D. B. (1999) Rapid automated molecular replacement by evolutionary search, *Acta Crystallogr., Sect. D: Biol. Crystallogr. 55* (Part 2), 484−491.
38. Brunger, A. T., Adams, P. D., Clore, G. M., DeLano, W. L., Gros, P., Grosse-Kunstleve, R. W., Jiang, J. S., Kuszewski, J., Nilges, M., Pannu, N. S., Read, R. J., Rice, L. M., Simonson, T., and Warren, G. L. (1998) Crystallography & NMR system: A new software suite for macromolecular structure determination, *Acta Crystallogr., Sect. D: Biol. Crystallogr. 54* (Part 5), 905−921.
39. Ramachandran, G. N., Ramakrishnan, C., and Sasisekharam, V. (1963) Stereochemistry of polypeptide chain configurations, *J. Mol. Biol. 7*, 95−99.
40. Kabsch, W. (1976) A solution for the best rotation to relate two sets of vectors, *Acta Crystallogr. A 32*, 922−923.
41. Kraulis, P. J. (1991) MOLSCRIPT: a program to produce both detailed and schematic plots of protein structures, *J. Appl. Crystallogr. 24*, 946−950.
42. Merritt, E. A., and Bacon, D. J. (1997) Raster3D: Photorealistic molecular graphics, *Methods Enzymol. 277*, 505−524.
43. Funahashi, J., Takano, K., and Yutani, K. (2001) Are the parameters of various stabilization factors estimated from mutant human lysozymes compatible with other proteins?, *Protein Eng. 14*, 127−134.
44. Connolly, M. L. (1993) The molecular surface package, *J. Mol. Graphics. 11*, 139−141.
45. Ogasahara, K., Hiraga, K., Ito, W., Miles, E. W., and Yutani, K. (1992) Origin of the mutual activation of the α and β_2 subunits in the $\alpha_2\beta_2$ complex of tryptophan synthasde.: Effect of alanine or glycine substitutions at proline residues in the α subunit, *J. Biol. Chem. 267*, 5222−5228.
46. Hiraga, K., and Yutani, K. (1997) Roles of hydrogen bonding residues in the interaction between the α and β subunits in the tryptophan synthase complex. Asn-104 of the α subunit is especially important, *J. Biol. Chem. 272*, 4935−4940.
47. Hiraga, K., and Yutani, K. (1996) A thermodynamic analysis of conformational change due to the $\alpha_2\beta_2$ complex formation of tryptophan synthase, *Eur J. Biochem. 240*, 63−70.
48. Nishio, K., Morimoto, Y., Ishizuka, M., Ogasahara, K., Tsukihara, T., and Yutani, K. (2005) Conformational changes in the α-subunit coupled to binding of the β_2-subunit of tryptophan synthase from *Escherichia coli*: Crystal structure of the tryptophan synthase α-subunit alone, *Biochemistry 44*, 1184−1192.
49. Nicholls, A., Sharp, K., and Honig, B. (1991) Protein folding and association: insights from the interfacial and thermodynamic properties of hydrocarbons, *Proteins 11*, 281−296.
50. Kirschner, K., Lane, A. N., and Strasser, A. W. (1991) Reciprocal communication between the lyase and synthase active sites of the tryptophan synthase bienzyme complex, *Biochemistry 30*, 472−478.
51. Anderson, K. S., Miles, E. W., and Johnson, K. A. (1991) Serine modulates substrate channeling in tryptophan synthase. A novel intersubunit triggering mechanism, *J. Biol. Chem. 266*, 8020−8033.
52. Raboni, S., Bettati, S., and Mozzarelli, A. (2005) Identification of the geometric requirements for allosteric communication between the alpha- and beta-subunits of tryptophan synthase, *J. Biol. Chem. 280*, 13450−13456.

BI050317H